

Efficient Time-Linearised TSD Computations Including the Effects of Shock-Generated Entropy, Vorticity and Shock Wave Motion

Eddie Ly

School of Mathematical & Geospatial Sciences

RMIT University

Melbourne, Australia

Jiro Nakamichi

Aviation Program Group

Japan Aerospace Exploration Agency

Tokyo, Japan

ABSTRACT

The effect of small perturbations on steady nonlinear transonic small disturbance flow-fields, in the context of two-dimensional flows governed by the general-frequency transonic small disturbance equation with nonreflecting far-field boundary conditions, is investigated. This paper presents a time-linearised time-domain solution method that includes effects due to the shock-generated entropy and vorticity and shock wave motions. The solution procedure correctly accounts for the small-amplitude shock wave motion due to small unsteady changes in the aerofoil boundary conditions, and correctly models a flow-field with embedded strong shock waves. Steady and first harmonic pressure distributions for the NACA 0003 aerofoil with a harmonically oscillating flap, and NACA 0012 aerofoil undergoing a sinusoidal pitching oscillation, are predicted and compared with the Euler results.

1.0 INTRODUCTION

Transonic flows are characterised by the presence of adjacent regions of subsonic and supersonic flow, usually accompanied by shock waves. In the past, there has been much activity in the development of computational methods for the analysis of time-linearised transonic flows. This activity was motivated by the need to supplement expensive and time consuming wind tunnel tests with an affordable and reliable alternative.

This paper presents a simple and fast scheme for computing time-linearised solutions to the general frequency transonic small disturbance (TSD) equation subject to nonreflecting far-field boundary conditions. The first author presented the time-linearised theory in Ly and Gear^(1,2), and has shown the importance of proper modeling of shock wave motion if one wants to obtain accurate time-linearised transonic solutions. The purpose of this paper is to present the modifications that have been recently incorporated into the time-linearised theory and existing potential code,

TranFlow2D, of Ly and Gear⁽²⁾ to enhance its capabilities to model

flowfields with embedded strong shock waves, so that Euler-like solutions can be obtained. The resulting time-linearised theory will be referred to as the modified time-linearised TSD (MTL-TSD) theory throughout this paper.

First modification is the inclusion of the shock-generated entropy and vorticity effects (Hafez and Lovell⁽³⁾, Whitlow *et al.*⁽⁴⁾, Batina⁽⁵⁾ and Dang and Chen⁽⁶⁾) to enhance the capability of *TranFlow2D* in simulating flowfields with embedded strong shock waves. The second modification involves a procedure, which we have referred to as the shock jump correction procedure (Ly and Gear⁽²⁾), that allows one to include the shock wave motion effects by correcting the solution values behind the shock wave, such that the time-linearised form of the shock jump condition will be satisfied.

We treat the unsteady flow as a small perturbation about a steady (mean) state. This results in a coupled flow problem for the steady and first-order unsteady reduced velocity potentials. The steady flow problem is governed by the usual nonlinear steady TSD equation (Ly and Gear⁽²⁾, Traci *et al.*^(7,8), Fung *et al.*⁽¹²⁾ and Ly *et al.*^(1,3)) and shock-generated entropy and vorticity effects are incorporated. The governing equation for the first-order unsteady reduced potential is linear, locally of mixed elliptic/hyperbolic type depending upon the nature of the steady-state solution, and solved in conjunction with the shock jump correction procedure. This will effectively correct the solution values behind the shock wave, which in turn introduces the shock wave motion effects into the time-linearised solution. In the closure, the validity of the present theory is verified by comparing the predicted results for the NACA 0003 aerofoil with a harmonically oscillating flap, and NACA 0012 aerofoil undergoing a sinusoidal pitching oscillation about quarter chord point, with those obtained from the NAL's Euler code. The comparisons show that the MTL-TSD theory has the capabilities to capture the flow characteristics shown in the Euler results.

2.0 GENERAL-FREQUENCY TSD EQUATION AND BOUNDARY CONDITIONS

The unsteady, isentropic and inviscid flow over a thin aerofoil is assumed to be governed by the general-frequency TSD equation,

which may be written in a convenient form as

$$M_\infty^2 \frac{\partial}{\partial t} (\phi_t + 2\phi_x) + \frac{\beta^2}{2\bar{u}} \frac{\partial}{\partial x} W^2 - \frac{\partial}{\partial z} \phi_z = 0 \quad (1)$$

where

$$W = \bar{u} - \phi_x \quad (2), (3), (4)$$

and $\phi_\lambda = \partial\phi/\partial x$, etc.

The spatial coordinates (x, z) , t and ϕ have been nondimensionalised by $\bar{u} c/U_\infty$ and $\frac{\beta^2}{\rho U_\infty^2}$, respectively. In nondimensional terms, the fluid velocity vector is given by $\mathbf{v} = (u, w) = \text{grad}(x + \phi)$. Here u denotes the value of ϕ_x at sonic condition, that is, where local Mach number is one.

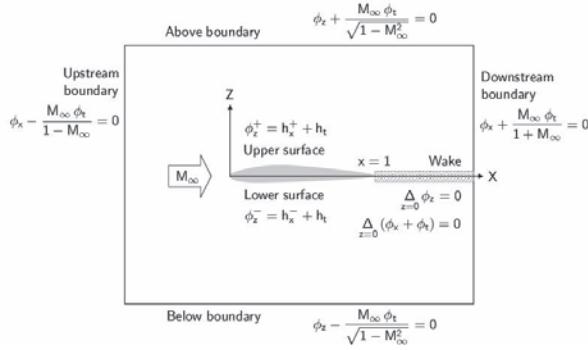


Figure 1. Boundary conditions.

Nonreflecting boundary conditions (Gear *et al.*⁽¹⁾ and Kwak⁽¹⁷⁾), derived from the theory of wave propagation, are employed at the far-field computational boundaries, and Kutta condition is satisfied at the trailing edge and pressure continuity condition is also satisfied in the wake region behind the aerofoil. The flow tangency boundary condition is imposed on a flat mean surface (approximation to the aerofoil) in terms of aerofoil slopes as depicted in Figure 1. The aerofoil lies on the $z = 0$ plane with the leading and trailing edges located at $x = 0$ (also the origin of the Cartesian coordinate system) and $x = 1$, respectively. Nonreflecting far-field boundary conditions are imposed at some finite distances and serve to simulate the disturbances that propagate outward from the aerofoil to infinity. Consequently, the far-field boundaries can be moved closer to the aerofoil. Any shock wave that exists in the flowfield must satisfy the shock jump condition (Fung *et al.*⁽¹²⁾ and Ly *et al.*⁽¹³⁾) derived from the conservation law form of Equation (1), namely,

$$M_\infty^2 \langle \phi_t + 2\phi_x \rangle \langle \phi_x \rangle \frac{d\Lambda}{dt} + \frac{\beta^2}{\bar{u}} \bar{W} \langle \phi_x \rangle^2 + \langle \phi_z \rangle^2 = 0 \quad (5)$$

together with the condition derived from the assumption of irrotationality,

$$\theta = - \frac{\langle \phi_z \rangle}{\langle \phi_x \rangle} \quad (6)$$

3.0 MODIFIED TIME-LINEARISED TSD THEORY

This section describes the time-linearisation process of the general-frequency TSD equation in time domain and the two modifications introduced into the inviscid theory.

3.1 Time-linearised time-domain formulation

In the time-linearisation process, we assume unsteady disturbances are small relative to a fixed mean state. This mean state is presumably represented by the nonlinear steady flowfield (Ly and Gear⁽²⁾, Traci *et al.*^(7,8) and Ly *et al.*⁽¹³⁾), and result in a coupled flow problem for the steady (ϕ) and first-order unsteady (ϕ_u) reduced potentials. The main dimensionless parameter governing unsteady flow is the reduced frequency number, k . The disturbance is assumed small, so that the aerofoil motion and reduced potential can be time-linearised as, to first-order approximations

$$h^\pm(x, t) = h_s^\pm(x) + h_u(x, t) \quad (7) \text{ and } (8)$$

$$\phi(x, z, t) = \phi_s(x, z) + \phi_u(x, z, t)$$

We define the mean potential by the steady-state potential obtained at the mean position of the aerofoil motion. This restriction ensures that the calculation of the first harmonics potential is accurate.

There are two advantages of time-linearising the reduced potential of the form shown in Equation (8):

1. Shock wave motion effects can be included in the time-linearised calculation, so that the solution within the shock trajectory will be correctly predicted.
2. There are no restrictions imposed on the mode of aerofoil motion that can be simulated, comparing to the harmonic decomposition of the following form

$$h^\pm(x, t) = h_s^\pm(x) + \Re \{ h_o(x) e^{ikt} \} \quad (9), (10)$$

$$\phi(x, z, t) = \phi_s(x, z) + \phi_o(x, z) e^{ikt}$$

where ϕ_o is a complex-valued oscillatory component of the reduced potential. To facilitate the use of high density of grid points surrounding the aerofoil, a smooth non-uniform computational mesh is constructed via an algebraic mapping process. In general terms, the mapping functions

$$\xi = \xi(x) \quad (11)$$

$$\zeta = \zeta(z) \quad (12)$$

Substituting approximations (7) and (8) into Equation (1) with the boundary conditions shown in Figure 1, and separating the steady and unsteady components, we find that ϕ_u satisfies the usual nonlinear steady TSD equation,

$$\frac{\beta^2}{2\bar{u}} \xi_x \frac{\partial}{\partial \xi} W_s^2 - \zeta_z \frac{\partial}{\partial \zeta} \zeta_z \frac{\partial \phi_s}{\partial \zeta} = 0 \quad (13)$$

where

$$W_s = \bar{u} - \xi_x \frac{\partial \phi_s}{\partial \xi} \quad (14)$$

Equation (13) is locally of elliptic/hyperbolic type representing subsonic/supersonic flow when W_s is positive/negative, and its solution contains discontinuous jumps that approximate steady shock waves. The required steady boundary conditions are those depicted in Figure 1 without the time-dependent terms and with ϕ_s replacing ϕ . While ϕ_u satisfies

$$M_\infty^2 \frac{\partial^2 \phi_u}{\partial t^2} + 2M_\infty^2 \frac{\partial}{\partial t} \xi_x \frac{\partial \phi_u}{\partial \xi} = \frac{\beta^2}{\bar{u}} \xi_x \frac{\partial}{\partial \xi} W_s \xi_x \frac{\partial \phi_u}{\partial \xi} + \zeta_z \frac{\partial}{\partial \zeta} \zeta_z \frac{\partial \phi_u}{\partial \zeta} \quad (15)$$

subject to the same far-field and wake boundary conditions of Figure 1, but with ϕ_u replacing ϕ and the following aerofoil boundary condition

$$\zeta_z^\pm \frac{\partial \phi_u^\pm}{\partial \zeta} = \xi_x \frac{\partial h_u}{\partial \xi} + \frac{\partial h_u}{\partial t} \quad (16)$$

Equation (15) is linear with respect to ϕ_u , and it is locally of the same mixed elliptic/hyperbolic type as Equation (13), depending upon the nature of the steady-state solution. The linearity of Equation (15) makes the computational effort required to obtain a solution much less than the effort required to obtain a solution of the full nonlinear TSD equation [Equation (1)].

The required solution for ϕ_s , which does not depend on ϕ_u , is solved independently, and is then used in the unsteady solution process to determine ϕ_u . This approach has the benefit that ϕ_s need not be regenerated for each unsteady boundary disturbance or reduced frequency of interest. Once ϕ is determined, the isentropic pressure coefficient can be determined from

$$\begin{aligned} C_p &= C_{ps} + C_{pu} \\ &= -2\xi_x \frac{\partial \phi_s}{\partial \xi} - 2 \left[\xi_x \frac{\partial \phi_u}{\partial \xi} + \frac{\partial \phi_u}{\partial t} \right] \end{aligned} \quad (17)$$

On the right side of Equation (17), the first term and terms inside the brackets correspond to C_{ps} and C_{pu} , respectively, and the critical pressure coefficient is defined by

$$C_p^* = -2\bar{u} \quad (18)$$

3.2 Inclusion of shock-generated entropy and vorticity effects

The shock-generated entropy and vorticity effects, similar to those reported by Hafez and Lovell⁽⁹⁾, Whitlow *et al.*⁽⁴⁾, Batina⁽⁵⁾ and Dang and Chen⁽⁶⁾, are incorporated into the steady analysis, so that flowfields with embedded strong shock waves can be simulated accurately. Rotational effects become influential when strong shock waves exist in the flowfield, since vorticity is generated due to the entropy changes along the shock. Such effects were not included in the conventional inviscid TSD theory, see Gear *et al.*⁽¹⁾, Ly and Gear⁽²⁾ and Ly *et al.*⁽¹³⁾, because of the irrotationality assumption necessary for the existence of a velocity potential. Therefore, when modelling such flowfield it is essential to include the shock-generated entropy and vorticity effects. We replace the streamwise flux of Equation (13) by an alternative flux, and rewrite the new steady governing equation with an artificial time derivative appended, so that the method of false transients can be applied (see Ly *et al.*^(13,18), Ly⁽¹⁴⁾ and Catherall⁽¹⁹⁾ for more details),

$$\frac{\partial \phi_s}{\partial \tau} = \frac{\beta^2}{2\bar{u}} \xi_x \frac{\partial}{\partial \xi} \hat{W}_s^2 - \zeta_z \frac{\partial}{\partial \zeta} \zeta_z \frac{\partial \phi_s}{\partial \zeta} \quad (19)$$

$$\hat{W}_s = \frac{\bar{u}}{\mu} - \frac{\mu(1 + \mu^2) \xi_x \frac{\partial \phi_s}{\partial \xi}}{1 + \mu^2 + \xi_x \frac{\partial \phi_s}{\partial \xi}} \quad (20), (21)$$

$$\mu = (1 + 2\bar{u})^{1/4}$$

In the modification to include vorticity effects, \mathbf{v} is treated as a sum of potential and rotational components, and the rotational component assumed to exist only in the region downstream of the shock wave. Since entropy is constant in steady flow, and assuming small shock curvature, the steady streamwise component of \mathbf{v} , namely u_s , for grid points behind the shock wave is modified to

$$u_s = 1 + \xi_x \frac{\partial \phi_s}{\partial \xi} - \ln \left[\frac{2\gamma M_n^2 - \gamma + 1}{\gamma + 1} \right]^{\frac{1}{\gamma(\gamma-1)M_n^2}} + \ln \left[\frac{(\gamma+1)M_n^2}{2 + (\gamma-1)M_n^2} \right]^{\frac{1}{(\gamma-1)M_n^2}} \quad (22)$$

The first two terms on the right side of Equation (22) represent the contribution from the inviscid model, and the last two terms are related to the production of shock-generated entropy. The entropy jump is a function of the normal Mach number upstream of the shock wave (Rankine-Hugoniot shock jump relation), and the shock wave location must be determined before the entropy jump can be computed. The present finite difference scheme uses a type-dependent finite differencing strategy (see Gear *et al.*⁽¹⁾, Engquist and Osher⁽²⁰⁾, Murman⁽²¹⁾ and Subsection 4.2) to capture shock waves and to properly treat the local subsonic and supersonic regions, thus the shock wave can easily be located. Consequently, the modified TSD theory will have a new steady governing equation given by Equation (19).

3.3 Inclusion of shock wave motion effects

In two-dimensional small-disturbance transonic flowfields, the shock waves that usually occur are nearly normal to the flow direction (Tijdeman⁽¹⁶⁾). Therefore, we can assume that if the steady flowfield has a shock wave, then this shock may be approximated by a normal shock wave. We computed the shock wave motion in conjunction with the solution to Equation (15). The shock wave motion effects are incorporated into the solution procedure by correcting the solution values behind the shock wave, such that the time-linearised form of the shock jump condition [Equation (5)] is satisfied. The shock wave motion is time-linearised (Ly and Gear⁽²⁾ and Fung *et al.*⁽¹²⁾) as, to first-order approximation and,

$$\Lambda(t) = \Lambda_s + \Lambda_u(t) \quad (23)$$

where Λ_s is the magnitude of the time-linearised shock motion. The reduced velocity potential at the shock wave is expanded via a Taylor series expansion about $\xi = \xi(\Lambda_s)$,

$$\phi(\Lambda(t), \zeta, t) = \phi(\Lambda_s, \zeta, t) + \Lambda_u \xi_x \frac{\partial \phi}{\partial \xi} + \frac{\Lambda_u^2}{2} \xi_x \frac{\partial}{\partial \xi} \xi_x \frac{\partial \phi}{\partial \xi} + \frac{\Lambda_u^3}{6} \xi_x \frac{\partial}{\partial \xi} \xi_x \frac{\partial}{\partial \xi} \xi_x \frac{\partial \phi}{\partial \xi} + \dots \quad (24)$$

threading the shock front and neglecting higher order terms in Λ_u , provides

$$\begin{aligned} \langle \phi_s(\Lambda_s, \zeta) \rangle &= 0 \\ \langle \phi_u(\Lambda_s, \zeta, t) \rangle &= \frac{1}{2} \Lambda_u \langle C_{ps} \rangle \end{aligned} \quad (25), (26)$$

In addition to the above relations, the shock wave speed relation is required, so that Λ_u can be computed once ϕ_u is known. Simplifying Equation (5) for normal shock waves, and making use of Equations (8) and (23) leads to $W_s = 0$ and the following time-linearised shock jump condition relations,

$$\begin{aligned} \frac{d\Lambda_u}{dt} &= \frac{\beta^2}{2\bar{u}M_\infty^2} \zeta_x \frac{\partial \phi_u}{\partial \xi} \\ \theta &= 0 \end{aligned} \quad (27), (28)$$

Equation (27) is integrated at the shock foot at each time level of the solution process.

4.0 NUMERICAL IMPLEMENTATION

4.1 Steady and unsteady finite difference based algorithms

The numerical solution procedure involves applying the method of false transients (Ly *et al.*^(13,18), Ly⁽¹⁴⁾ and Catherall⁽¹⁹⁾) to solve Equation (19) for ϕ_s , and noniterative alternating directional implicit (ADI) method in conjunction with the shock jump correction procedure to solve Equation (15) for ϕ_u .

The ADI method computes the solution by marching forward in time from its initial steady-state to subsequent time levels in a two-step process from time-level t_n to t_{n+1} . Intermediate values, $\psi(\xi, \zeta, \delta)$, are computed at the midpoint of each time interval. We first write Equation (15) and all associated unsteady boundary conditions at time-level $t_{n+1/2}$ which is the midpoint of time levels t_n and t_{n+1} , and evaluate ψ_t by the trapezoidal rule and ψ_u by a second-order accurate nonstandard forward difference rule involving solution values from time-level t_{n-2} to t_{n+1} . The vertical derivative is averaged between the values at time-level tn and $tn+1$. Equation (15) is then split into two half equations with ψ computed along the $\zeta = \text{constant}$ lines of the computational grid in the first half step, and then along the $\xi = \text{constant}$ lines in the second half step for ϕ^{n+1}_u . It is necessary to introduce boundary values for ψ , which we will not discuss here, that are compatible with the interior algorithms corresponding to the two half equations, so that a global truncation error of second-order in time can be attained. Equation (26) is differentiated with respect to time at time-level $t_{n+1/2}$, and replacing the time-linearised shock wave speed term with Equation (27). The final finite difference scheme being globally second-order accurate in the spatial and time dimensions, except in the flow regions where shock wave motion occurs, in which case the time dimension is reduced to first-order accuracy. In the first half-step we solve for ψ along $\zeta = \text{constant}$ lines using

$$\frac{2M_\infty^2}{\Delta t} \xi_x \frac{\partial \psi}{\partial \xi} - \frac{\beta^2}{\bar{u}} \xi_x \frac{\partial}{\partial \xi} W_s \xi_x \frac{\partial \psi}{\partial \xi} = \frac{2M_\infty^2}{\Delta t} \xi_x \frac{\partial \phi_u^n}{\partial \xi} + \zeta_z \frac{\partial}{\partial \zeta} \zeta_z \frac{\partial \phi_u^n}{\partial \zeta} \quad (29)$$

in conjunction with the computation of new ψ value behind the shock wave,

$$\langle \psi \rangle = \langle \phi_u^n \rangle + \frac{\Delta t \beta^2}{4\bar{u}M_\infty^2} \zeta_x \frac{\partial \phi_u^n}{\partial \xi} \langle C_{ps} \rangle \quad (30)$$

With ψ determined, the second half-step follows, computing ϕ_{n+1}_u along $\xi = \text{constant}$ lines using

$$\begin{aligned} \frac{3M_\infty^2}{2(\Delta t)^2} \phi_u^{n+1} + \frac{2M_\infty^2}{\Delta t} \xi_x \frac{\partial \phi_u^{n+1}}{\partial \xi} - \frac{1}{2} \zeta_z \frac{\partial}{\partial \zeta} \zeta_z \frac{\partial \phi_u^{n+1}}{\partial \zeta} \\ = \frac{M_\infty^2}{2(\Delta t)^2} (7\phi_u^n - 5\phi_u^{n-1} + \phi_u^{n-2}) + \frac{2M_\infty^2}{\Delta t} \xi_x \frac{\partial \psi}{\partial \xi} - \frac{1}{2} \zeta_z \frac{\partial}{\partial \zeta} \zeta_z \frac{\partial \phi_u^n}{\partial \zeta} \end{aligned} \quad (31)$$

in conjunction with the updated $\langle \phi_u^n \rangle$ values along the shock wave,

$$\langle \phi_u^{n+1} \rangle = \langle \psi \rangle \quad (32)$$

4.2 Spatial discretisation

In the finite difference schemes, the first streamwise and vertical derivatives are differenced using standard second-order accurate upwind and central rules, respectively. While a second-order accurate Engquist-Osher type-dependent difference rule (Gear *et al.*⁽¹⁾ and Engquist and Osher⁽²⁰⁾) is used for the second streamwise derivatives. As the flow changes from subsonic to supersonic, Engquist-Osher type-dependent operators smoothly change from a central difference rule (to account for the domain of dependence of elliptic region) to an upwind difference rule (to account for the absence of downstream influence in hyperbolic region). This ensures a smooth transition from subsonic to supersonic flow. Hence, entropy violating decompression shock waves will not develop. As the flow changes from supersonic to subsonic, the Engquist-Osher type-dependent operators change to an appropriate shock point operator (Murman⁽²¹⁾), and for the computation of ϕ_u the shock jump correction is implemented at this stage. The correction procedure disregards the actual variation in ϕ_u , and thus, is only able to account for small-amplitude shock wave motions.

Table 1: Case studies.

| Motion Mode | Case | Aerofoil | M_∞ | k | α_m | $\Delta\alpha$ | δ_m | $\Delta\delta$ | Figs. |
|----------------------|------|-----------|------------|-------|------------|----------------|------------|----------------|-------|
| Flap oscillation | 1 | NACA 0003 | 0.93 | 0.125 | 0 | 0 | 0 | 1 | 2,3 |
| | 2 | NACA 0003 | 0.93 | 0.25 | 0 | 0 | 0 | 1 | 2,3 |
| Pitching oscillation | 3 | NACA 0012 | 0.84 | 0.25 | 0 | 0.25 | 0 | 0 | 4,5 |
| | 4 | NACA 0012 | 0.84 | 0.25 | 0 | 0.5 | 0 | 0 | 4,5 |
| | 5 | NACA 0012 | 0.8 | 0.25 | 1.25 | 0.25 | 0 | 0 | 6,7 |

5.0 ASSESSMENT OF MODIFIED THEORY

The first author has confirmed the validity of the time-linearised calculations by demonstrating that the time-linearised theory is capable of generating results which are similar to that predicted by the nonlinear scheme of Gear *et al.*⁽¹⁾ (solving the full nonlinear TSD equation) for transonic flows over an aerofoil in small-amplitude motions, see Ly and Gear⁽²⁾ for more details. In this section we apply

the MTL-TSD theory and code (version 2 of *TranFlow2D*) to compute the time-linearised results for the cases tabulated in Table 1, and to show that Euler-like solutions can be obtained by comparing present results with those predicted by the JAXA's Euler code (details on the Euler solver can be found in Kheirandish *et al.*⁽²²⁾ and Nakamichi and Kheirandish⁽²³⁾). All unsteady results become periodic within four cycles of oscillation, with the last cycle providing the estimate of the unsteady pressure distributions. In addition, linear results obtained from solving the unsteady compressible subsonic small disturbance equation are presented for reference, so that the pressure peaks generated by the shock waves (shown in the transonic results which follow) can easily be distinguished. All angles are positive for trailing edge down, and moments are positive for nose up, taken about the aerofoil quarter-chord point.

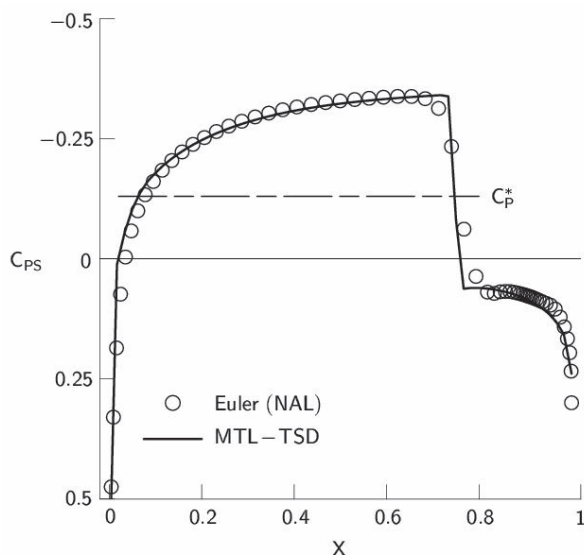


Figure 2. Comparison of steady pressure distributions for the NACA 0003 aerofoil with a 9.6% chord flap at $M_\infty=0.93$ and $\delta_m=0$ deg.

5.1 NACA 0003 aerofoil results

The first two cases consider flows over an NACA 0003 aerofoil with a harmonically oscillating 9.6% chord flap (flap hinge located at 90.4% chord). The results are compared in Figures 2 and 3. The steady pressure distribution corresponds reasonably well with the Euler result as shown in Figure 2, except for the very small regions adjacent to the shock wave located at 74.7% chord, where the MTL-TSD theory gives a much sharper shock profile. The steady shock wave strength is also well predicted, with the jump in C_{ps} approximating the steady shock wave and $C_{ps}/C_p^* > 1$ indicating locally supersonic point. To assist in the comparison of the unsteady results, an approximating trace of the pressure responses in the form of a truncated Fourier series with only one harmonic is fitted to the result by a least squares procedure. The fitted parameters are then written in complex-valued form, so that the real (in-phase) and imaginary (out-phase) parts of ΔC_p per unit of flap deflection, where $\Delta C_p = (\Delta C_p^+ - \Delta C_p^-) \Delta \delta$ can be extracted and plotted as shown in Figure 3 for reduced frequencies of

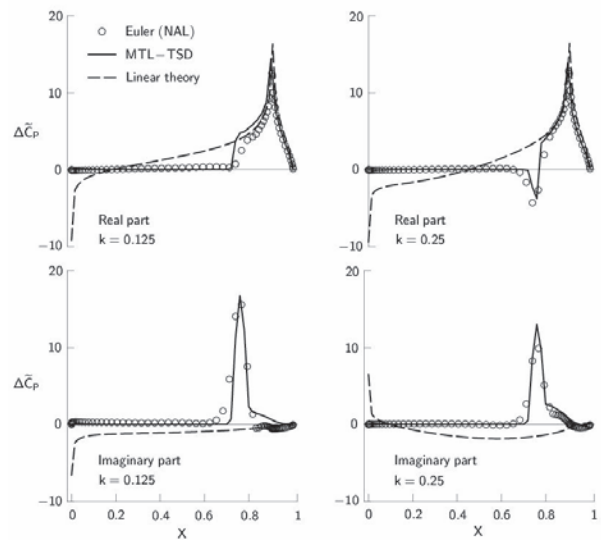


Figure 3. Comparison between the Euler, MTL-TSD and linear results for the NACA0003 aerofoil with a harmonically oscillating 9.6% chord flap at $M_\infty=0.93$, $k=0.125$ and 0.25 , $\delta_m=0$ deg and $\Delta\delta=1$ deg.

125 and 0.25. The positive peak of the real pressure part is caused by the changes in aerofoil slopes across the flap hinge. While the peak of the imaginary part is due to the existence of steady shock wave, leading to the observation that the embedded shock waves in the steady flowfield require corresponding shock waves in the unsteady perturbation flowfield, which in effect result in harmonic changes in shock wave strength. Also noting that the comparison of the imaginary part behind the shock wave for case 2 ($k=0.25$) is much better than that of case 1 ($k=0.125$).

The amplitude of shock excursion is proportional to $1/k$, and so, the flow region influenced by the shock wave motion for high-frequency flows is small, which suits the application of the time-linearised methods. Hence, resulting in the improvement of the imaginary part of the solution. If the time-linearised theory is formulated in the frequency domain, one can in fact show that the amplitude of shock excursion is proportional $1/k$ via the following relation,

$$\Lambda_u = -\Re \left\{ \frac{i(\gamma+1)}{2k} \overline{\xi_x \frac{\partial \phi_o}{\partial \xi}} e^{ikt} \right\} \quad (33)$$

where ϕ_u and ϕ_o are related by

$$\phi_u = \Re \left\{ \phi_o e^{ikt} \right\} \quad (34)$$

Even though the MTL-TSD theory slightly over predicts the pressure perturbation peaks, the comparison is good in general, since both methods give the same trend of pressure perturbation distributions along the aerofoil surfaces. Furthermore, all pressure peaks are correctly captured, particularly the negative peak appearing in Figure 3 for $k=$

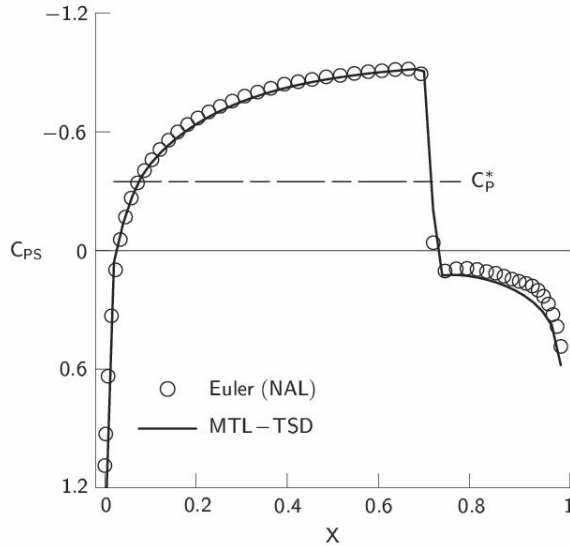


Figure 4. Comparison of steady pressure distributions for the NACA 0012 aerofoil at $M_\infty = 0.84$ and $\alpha_m = 0$ deg.

0.25. The authors suspect that the small discrepancies in the comparison are due to the amount of incorporated (numerical) entropy being not exactly the same as the true value, and due to the fact that the unsteady flowfield is treated as a small perturbation about the steady flowfield instead of the true mean flowfield. However, the discrepancies in the shock region being small indicate that taking the steady flowfield and steady shock position to represent the mean flowfield and mean shock position, respectively, is reasonable. The mean shock position determined by the Euler code is about 75.6% chord, which is very close to the steady shock position predicted by the present MTL-TSD theory of 74.7% chord, a difference in distance of less than 1% chord. Note that it is essential to have a well defined steady (mean) flowfield, because a good agreement on the steady pressure distribution is a prerequisite to obtain a good agreement on the unsteady pressure distribution for the time-linearised computations. In future work we may consider taking the mean flowfield

from a complete nonlinear unsteady solution of Equation (1) for cases where the steady and mean shock waves are not close to each other. The linear theory, as expected, is only able to capture the pressure peaks due to the flap hinge.

5.2 NACA 0012 aerofoil results

The next three cases are for flows over an NACA 0012 aerofoil undergoing a sinusoidal pitching oscillation about quarter-chord point, and the results are compared in Figures 4 to 7. The steady part of cases 3 and 4 is also studied by Whitlow *et al.*⁽⁴⁾ and Fuglsang and Williams⁽²⁰⁾, and the steady part of case 5 is an AGARD (Advisory Group for Aerospace Research and Development) test case for assessment of inviscid flow methods. The comparison of the

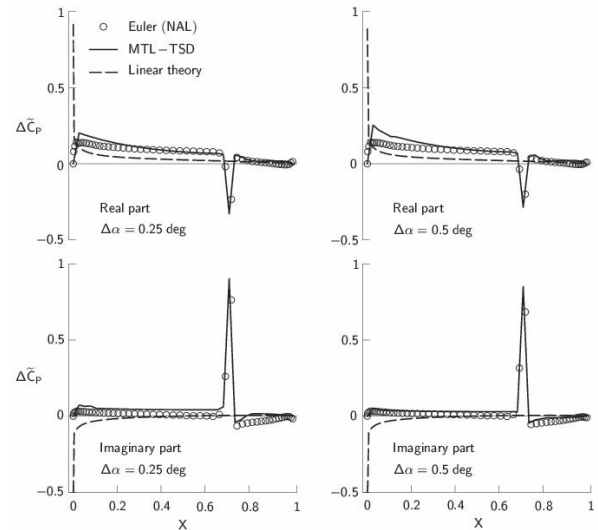


Figure 5. Comparison between the Euler, MTL-TSD and linear results for the NACA0012 aerofoil undergoing a sinusoidal pitching oscillation about quarter-chord point at $M_\infty = 0.84$, $k = 0.25$, $\alpha_m = 0$ deg and $\Delta\alpha = 0.25$ and 0.5 deg.

steady pressure distributions in Figures 4 and 6 is exceptional good, specifically in the accurate prediction of both the shock wave positions and strengths.

The perturbation pressure for the NACA 0012 aerofoil cases is extracted based on the following formula,

$$\Delta \tilde{C}_p = \frac{ik}{\pi \Delta \alpha} \oint C_p e^{ikt} dt \quad (35)$$

The MTL-TSD theory is able to capture the trend of the pressure distributions determined by the Euler theory (i.e. giving the same signs of the real and imaginary parts), but the unsteady results are usually slightly over predicted, see Figures 5 and 7.

Since the NACA 0012 aerofoil has no flap or moveable lifting surface where the aerofoil slopes change rapidly, the sharp pressure peaks shown in these plots are due to the shock wave only, and again, are well captured by the present theory. The steady shock positions are located very close to the mean locations, thus increasing the accuracy of the present results. The Euler method employs a body conformed dynamic grid system (Kheirandish *et al.*⁽²²⁾ and Nakamichi and Kheirandish⁽²³⁾), in which a new grid configuration is generated at each time level corresponding to the changes in the aerofoil position. While the present theory uses a stationary grid system with the flow tangency boundary condition imposed on a flat mean surface (approximation to the actual aerofoil) in terms of aerofoil slopes. Because of the

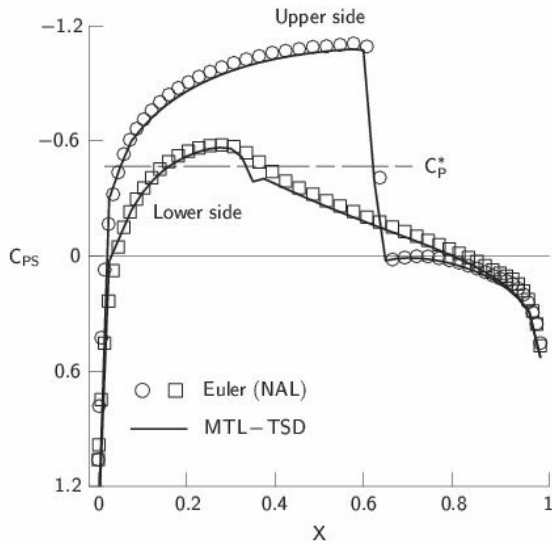


Figure 6. Comparison of steady pressure distributions for the NACA 0012 aerofoil at $M_\infty = 0.8$ and $\alpha_m = 1.25$ deg.

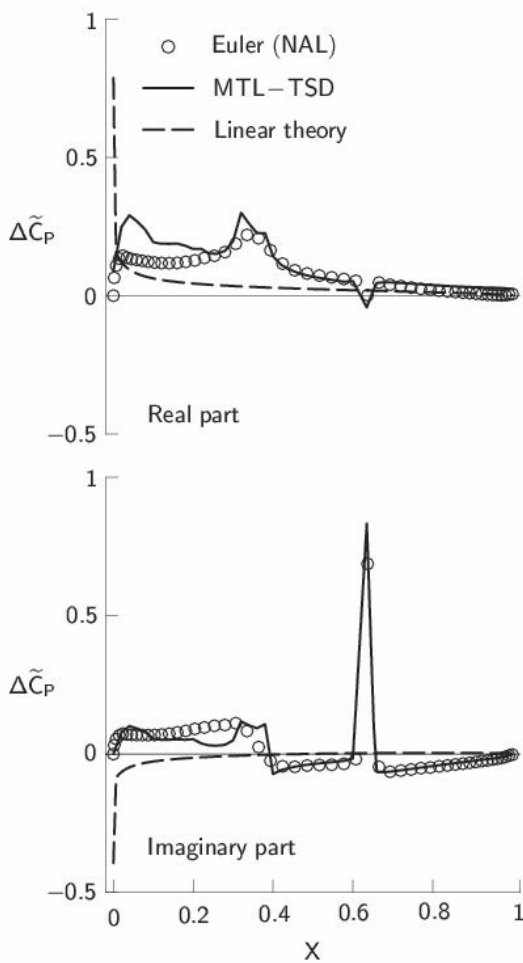


Figure 7. Comparison between Euler, MTL-TSD and linear results for NACA0012 aerofoil in a sinusoidal pitching oscillation about quarter-chord point at $M_\infty = 0.8$, $k = 0.25$, $\alpha_m = 1.25$ deg and $\Delta\alpha = 0.25$ deg.

different grid systems, the authors expected some discrepancies to

occur around the aerofoil nose. The discrepancy occurs only for the real pressure part, and becomes large for increasingly large maximum angle of attack. For example, in Figure 5 the discrepancy for case 4 is larger than that of case 3, since the angle of attack can reach upto 0.5 deg in case 4 compared to 0.25 deg in case 3. Similarly, Figure 7 shows much larger discrepancy for case 5 where the maximum angle of attack is 1.5 deg. This observation is consistent with the expectation that the distribution of the real (in-phase part) depends on the aerofoil profile and motion, since if comparing to cases 1 and 2 where only the flap that moves and 90.4% of the aerofoil is stationary, no such discrepancies occur around the aerofoil nose. The small peaks that appear in Figure 7 around 30 to 40% chord are generated by the vortex development in this region. Again, the MTL-TSD method captured such flow phenomenon remarkably well.

6.0 CONCLUDING REMARKS

An effective treatment of unsteady transonic flows, with moving shock waves, as a small perturbation about the steady (mean) flowfield was described. The solution method, in conjunction with the shock jump correction procedure and the inclusion of shockgenerated entropy and vorticity effects, has successfully produced accurate time-linearised time-domain solutions for transonic flows with embedded strong shock waves. The modifications made to the inviscid TSD theory leads to the development of a second version of *TranFlow2D* code. Solutions can be obtained in an acceptable turn-around time on current high performance personal computers, hence making it an ideal tool for performing two-dimensional transonic aeroelastic analysis and for students to experience numerical aerodynamic computations. Based on the present study, we obtained the following conclusions:

1. The satisfactory correlation of the results demonstrated that the presented theory is capable of predicting unsteady transonic flow with embedded strong shock waves.
2. The presented time-linearised formulation illustrated the importance of proper modeling of the shock wave motion in order to obtain accurate time-linearised transonic solutions.
3. The theory has been demonstrated to be successful, in a sense that it could be used to provide input for aeroelastic computations for which only infinitesimal magnitude motions need be considered.
4. In future work we may consider taking the mean flowfield from a complete nonlinear unsteady solution of the general-frequency TSD equation for cases where the steady and mean shock waves are not close to each other.
5. There is a future potential for a three-dimensional version as a fast method to be used for flutter predictions.

REFERENCES

[1] Gear, J. A., Ly, E. and Phillips, N. J. T. Time marching finite difference solution of the modified transonic small disturbance equation, Proceedings of the 8th Biennial Computational Techniques and Applications Conference (CTAC97), Australian and New Zealand

- Industrial and Applied Mathematics (ANZIAM), Adelaide, Australia, 29 Sep.–1 Oct. 1997, pp. 209–216.
- [2] Ly, E. and Gear, J. A. Time-linearized transonic computations including shock wave motion effects, *Journal of Aircraft*, Nov/Dec. 2002, Vol. 39, No. 6, pp. 964–972.
- [3] Hafez, M. and Lovell, D. Entropy and vorticity corrections for transonic flows, *AIAA Paper 83-1926*, July 1983.
- [4] Whitlow, W., Jr., Hafez, M. M. and Osher, S. J. An entropy correction method for unsteady full potential flows with strong shocks, *Journal of Fluids and Structures*, 1987, Vol. 1, pp. 401–414.
- [5] Batina, J. T. Unsteady transonic small-disturbance theory including entropy and vorticity effects, *Journal of Aircraft*, 1989, Vol. 26, No. 6, pp. 531–538.
- [6] Dang, T. Q. and Chen, L. T. An Euler correction method for two- and three dimensional transonic flows, *AIAA Paper 87-0522*, 1987.
- [7] Traci, R. M., Albano, E. D. and Farr, J. L., Jr. Small disturbance transonic flows about oscillating airfoils and planar wings, *AFFDL TR-75-100*, Air Force Flight Dynamics Lab., Wright-Patterson AFB, OH, USA, Aug. 1975.
- [8] Traci, R. M., Albano, E. D. and Farr, J. L., Jr. Perturbation method for transonic flows about oscillating airfoils, *AIAA Journal*, 1976, Vol. 14, No. 9, pp. 1258–1265.
- [9] Schippers, H. and Hounjet, M. H. L. Two complementary approaches to transonic potential flow about oscillating airfoils, *Journal of Aircraft*, 1988, Vol. 25, No. 5, pp. 395–398.
- [10] Hounjet, M. H. L. NLR inviscid transonic unsteady loads prediction methods in aeroelasticity, *Transonic Unsteady Aerodynamics and Aeroelasticity*, Paper CP-507, AGARD, March 1992, pp. 12.1–12.16. [11] Greco, P. C., Lan, C. E. and Lim, T. W. Frequency domain unsteady transonic aerodynamics for flutter and limit cycle oscillation prediction, *AIAA Paper 97-0835*, Jan. 1997.
- [12] Fung, K. Y., Yu, N. J. and Seebass, R. Small unsteady perturbations in transonic flows, *AIAA Journal*, 1978, Vol. 16, No. 8, pp. 815–822.
- [13] Ly, E., Gear, J. A. and Phillips, N. J. T. Simulated shock motion using a timelinerised transonic code, *Proceedings of the 3rd Biennial Engineering Mathematics and Applications Conference (EMAC98)*, The Institution of Engineers of Australia and Australian and New Zealand Industrial and Applied Mathematics (ANZIAM), Adelaide, Australia, 13–16 July 1998, pp. 331–334.
- [14] Ly, E. Improved approximate factorisation algorithm for the steady subsonic and transonic flow over an aircraft wing, *Proceedings of the 21st Congress of the International Council of the Aeronautical Sciences (ICAS 1998)*, AIAA and ICAS, Melbourne, Australia, 13–18 Sep. 1998, Paper A98-31699.
- [15] Batina, J. T. Unsteady transonic algorithm improvements for realistic aircraft applications, *Journal of Aircraft*, 1989, Vol. 26, No. 2, pp. 131–139.
- [16] Tijdeman, H. Investigations of the transonic flow around oscillating airfoils, *NLR TR 77090 U*, National Aerospace Lab. NLR, Amsterdam, The Netherlands, Oct. 1977.
- [17] Kwak, D. Nonreflecting far-field boundary conditions for unsteady transonic flow computation, *AIAA Journal*, 1981, Vol. 19, No. 11, pp. 1401–1407.
- [18] Ly, E., Gear, J. A. and Phillips, N. J. T. Improved approximate factorisation algorithm, *Proceedings of the 8th Biennial Computational Techniques and Applications Conference (CTAC97)*, Australian and New Zealand Industrial and Applied Mathematics (ANZIAM), Adelaide, Australia, 29 Sep.–1 Oct. 1997, pp. 393–400.
- [19] Catherall, D. Optimum approximate-factorization schemes for two-dimensional steady potential flows, *AIAA Journal*, 1982, Vol. 20, No. 8, pp. 1057–1063.
- [20] Engquist, B. and Osher, S. Stable and entropy satisfying approximations for transonic flow calculations, *Mathematics of Computation*, 1980, Vol. 34, No. 149, pp. 45–75.
- [21] Murman, E. M. Analysis of embedded shock waves calculated by relaxation methods, *AIAA Journal*, 1974, Vol. 12, No. 5, pp. 626–633.
- [22] Kheirandish, H. R., Goro, B. and Nakamichi, J. Numerical investigation of flutter, *International Journal of Computational Fluid Dynamics*, 1999, Vol. 12, pp. 279–290.
- [23] Nakamichi, J. and Kheirandish, H. R. Nonlinear flutter simulation of NAL non-powered SST experimental airplane and related wind tunnel tests, *CEAS/AIAA/AIAE International Forum on Aeroelasticity and Structural Dynamics*, Madrid, Spain, April 2001.
- [24] Fuglsang, D. F. and Williams, M. H. Non-isentropic unsteady transonic small disturbance theory, *AIAA Paper 85-0600*, April 1985.